

# Bayesian Optimisation of Intermittent Wall Blowing for Drag Reduction of a Spatially Evolving Turbulent Boundary Layer

O. A. Mahfoze, S. Laizet and A. Wynn  
Corresponding author: s.laizet@imperial.ac.uk

Department of Aeronautics, Imperial College London, London, SW7 2AZ, UK.

**Abstract:** A Bayesian Optimisation framework in conjunction with Direct Numerical Simulation (DNS) of spatially developing turbulent boundary layers (TBL) is used to study the potential of vertical wall blowing to reduce skin-friction drag but also to generate net-power saving. In order to obtain realistic values for the power needed to supply the wall blowing, the experimental data of Kornilov and Boiko [1] are used as well as the averaged friction coefficient over a large extent of the computational domain. For the present study it is found that after 18 DNS simulations, corresponding to 18 iterates of the Bayesian Optimisation scheme, the optimum strategy achieves a net-power saving of 5% via uniform blowing with moderate intensity (0.29% of the freestream velocity). It is found that it is possible to generate substantial drag reduction. However, this is associated with power losses (up to 20% net-energy loss with an average of 19% of drag reduction and values up to 60% locally). A Fukagata-Iwamoto-Kasagi (FIK) analysis shows two different mechanisms responsible for the drag reduction over and downstream of the blowing region. The reduction of the friction coefficient is associated with the FIK convection term over the blowing region, and the TIK spatial development term downstream of the blowing region.

*Keywords:* Computational Fluid Dynamics, Turbulent Boundary Layer, Drag Reduction, Bayesian Optimisation, Direct Numerical Simulations.

## 1 Introduction

Drag-reducing flow control is a topic of great interest due to its importance in many engineering applications. As an example, just a 3% reduction in the skin-friction of a long-range commercial aircraft would save £1.2m in jet fuel per aircraft per year and prevent the annual release of 3,000 tonnes of carbon dioxide. Despite many decades of extensive research, a practical and affordable method for skin-friction drag reduction is yet to be found and implemented in real-world applications. Various strategies, which includes polymer additives, riblets, vibrators, actuators, microelectromechanical systems, gas microbubbles, hydrophobic coating and large eddy breakup devices have been developed in the last decades to reduce skin-friction drag. Adding additives to a liquid flow, for instance, can reduce skin-friction drag by more than 70%, yielding a phenomenon known as Maximum-Drag-Reduction (MDR) (Graham [2]). For air flows, however, the energy expenditure of typical active drag reduction strategies can be very high, often leading to net-energy loss even if substantial skin-friction drag reduction is obtained (Quadrio and Ricco [3]).

In the present work we focus on the spatial development of a zero pressure gradient turbulent boundary layer and the resulting wall friction after control has been applied locally using vertical wall-blowing as a drag-reducing strategy. Mass flow injection from a surface is not new and can be traced back to the 40's with surface cooling studies by Dawes and Wheeler [4] and Mickley et al. [5]. Rubesin [6] and Torii et al. [7] developed analytical formulas for the calculation of the heat transfer and skin-drag coefficients under wall transpiration conditions which were later confirmed experimentally by Simpson et al. [8] with measurements to analyse and model the turbulent momentum and heat transport in the presence of injection and suction. Sumitani and Kasagi [9] performed Direct Numerical Simulations (DNS) of a turbulent channel flow with low-intensity (0.1% of the free stream velocity) uniform wall injection. They observed more than 10% drag reduction and concluded that higher intensities for the wall injection could lead to larger drag reduction. A DNS of a spatially developing turbulent boundary layer was performed in Kim et al. [10] to examine the characteristics of wall pressure fluctuations after the sudden application of wall blowing or suction. It was found that wall pressure fluctuations are more affected by blowing than by suction. For both blowing and suction, the small scale of wall pressure fluctuations reacts in a short downstream distance to after the blowing, whereas the large scale recovers slowly farther downstream. Experimental investigations using a blowing technique called the Microblowing Technique (MBT) have showed that it is possible to reduce turbulent skin friction by more than 50% in subsonic flow and more than 80% in supersonic flow (Hwang [11, 12]). However, the authors conclude that the main challenge is related to the blowing air resources which can be very substantial. Based on the parametric study of Hwang [12], and with the help of new advanced drilling technology, Kornilov and Boiko [1] designed micro-drilled surface and reported a reduction of the shear stress by more than 70%. Thanks to a detailed investigation of boundary-layer characteristics over the permeable surface, they managed to make real-time decisions for the experiment setup refinement to achieve the maximum efficiency of the control method under study. The estimated net-energy saving was only 5% due to the energy expenditure of the blowing system. Interestingly, they observed that the friction coefficient downstream of the blowing region only relaxes to its canonical value after a significant distance. This indicates the possibility of employing spatially-discontinuous blowing to achieve comparable drag reduction with less blowing power, as reported in Kornilov and Boiko [13].

Fukagata et al. [14] derived a simple expression which can explain the skin-friction drag in wall-bounded turbulent flows: the local skin friction can be decomposed into four parts, laminar, turbulent, inhomogeneous and transient components, the second of which is a weighted integral of the Reynolds stress distribution. This so-called FIK identity can be used to investigate drag reduction techniques. Note that for spatially evolving flows, this identity has the contributions from boundary layer thickness, the Reynolds shear stress, mean wall-normal convection, and spatial development. The simulations of Kametani and Fukagata [15] and Kametani et al. [16] showed that uniform suction can suppress turbulence but increases the drag, while uniform blowing can enhance turbulence but reduce shear stress. Their FIK analysis revealed the presence of pressure gradients near the edges of the suction/blowing area. These numerical studies also showed that the efficiency of the control increases with widening the streamwise length of the control section. More recently, DNS of a turbulent boundary layer with a low-intensity vertical wall-blowing control region have shown a local maximum skin-friction drag reduction of 60%, which persists to tens of boundary-layer thicknesses downstream of the control (Stroh et al. [17]). A series of Large-Eddy Simulations (LES) of spatially evolving turbulent boundary layers with vertical wall-blowing were performed in Kametani et al. [18] with a special focus on the effect of intermittent (separated in streamwise direction) blowing sections. A net-energy saving rate of around 18% was reported and a FIK study showed that the distribution of all components over each blowing section has similar trends, resulting in similar averaged values over the whole control region.

Employing a reliable optimisation method to determine the optimal parameters of a vertical wall-blowing control technique could potentially lead to substantial net-energy saving. Bayesian Optimisation (BO) is a derivative-free algorithm that works efficiently with expensive non-convex objective functions (Gelbart et al. [19]). BO plays a prominent role in efficiently optimising the parameters of machine learning algorithms, such as Neural Networks, with superior performance when compared to more standard approaches (Snoek et al. [20], Brochu et al. [21]). BO is yet to be used for fluid flow problems and very few studies combining DNS/LES and BO have been published to date. Talnikar et al. [22] developed a parallel Bayesian Optimisation algorithm for LES to minimize drag in a turbulent channel flow and to design the trailing edge of a turbine blade to reduce turbulent heat transfer and pressure loss. They managed to simultaneously run several simulations for their optimisation study, taking advantages of the concurrency offered by supercomputers.

In the present study, DNS of spatially evolving turbulent boundary layers are performed in order to investigate the potential of a Bayesian Optimisation algorithm to achieve net-power saving using intermittent vertical wall-blowing as a technique to reduce skin-friction drag. Unlike the majority of numerical studies where idealized situations are assumed, energy savings are evaluated by taking into account the hydraulic and mechanical loss of the blowing system, using the experimental data of Kornilov and Boiko [1]. For this first study, and for simplicity, only three blowing parameters are optimised to achieve maximum net-energy saving. Furthermore, the FIK identity is used to investigate in details the mechanism of the drag reduction.

## 2 Numerical Methods

The incompressible NavierStokes equations are solved using a recent version of the high-order flow solver `Incompact3d` (see [www.incompact3d.com](http://www.incompact3d.com)), adapted to parallel supercomputers using a powerful two-dimensional (2D) domain decomposition strategy (Laizet and Li [23]). This solver is based on sixth-order finite-difference schemes on a Cartesian mesh for the spatial discretization and a semi-implicit time advancement for the viscous terms. To treat the incompressibility condition, a fractional step method requires solution of a Poisson equation, fully solved in spectral space via the use of relevant 3D Fast Fourier transforms. Combined with the concept of the modified wave number (Lele [24]), this direct (i.e. non-iterative) technique allows the implementation of the divergence-free condition up to machine accuracy. A partially staggered mesh is used where the pressure mesh is shifted by a half-mesh from the velocity mesh in each direction. This type of mesh organization leads to more physically realistic pressure fields with no spurious oscillations. More details about the code can be found in Laizet and Lamballais [25]. `Incompact3d` has been recently used for DNS of TBL (Diaz-Daniel et al. [26, 27]), including comparison of wall-shear stress statistics and energy budget with the reference data of Schlatter and Örlü [28], Jiménez et al. [29].

The present simulations are performed for a domain size  $L_x \times L_y \times L_z = 750\delta_0 \times 40\delta_0 \times 15\delta_0$  discretized with  $n_x \times n_y \times n_z = 3073 \times 321 \times 128$  mesh nodes in the streamwise, normal, and the spanwise directions, respectively. Here,  $\delta_0$  is the boundary layer thickness at the inlet. A laminar Blasius boundary layer is prescribed at the inlet boundary condition in the streamwise direction, with a Reynolds number  $Re_\theta = U_\infty\theta/\nu = 170$  based on the momentum thickness  $\theta$  and the free-stream velocity  $U_\infty$ . A 1D convection equation is solved for the outlet boundary condition, where the Reynolds number reaches  $Re_\theta = 1850$ . In the spanwise direction, the boundary conditions are periodic while an homogeneous Neumann condition is imposed on the three velocity components at the top of the domain. The mesh is uniformly spaced in the streamwise and the spanwise directions, and is stretched towards in the wall normal direction. The resolution in wall units for  $Re_\theta = 365$

is  $\Delta x^+ = 0.84$ ,  $0.027 \leq \Delta y^+ \leq 6.8$  and  $\Delta z^+ = 0.4$ . The simulation time step is  $\Delta T = 0.008 \frac{\delta_0}{U_\infty}$ . The dimensions with superscript  $+$  are normalized with the local shear-velocity  $u_\tau$ . Turbulent conditions are triggered with the tripping method designed by Schlatter and Örlü [28], using the optimal parameters described by these authors. The tripping region is located at  $x = 3.5\delta_0$  and occupies the whole spanwise extent. Figure 1 illustrates the computational domain and the control region. Local uniform blowing  $v_w$  is applied through an inhomogeneous wall-boundary condition for the normal velocity.

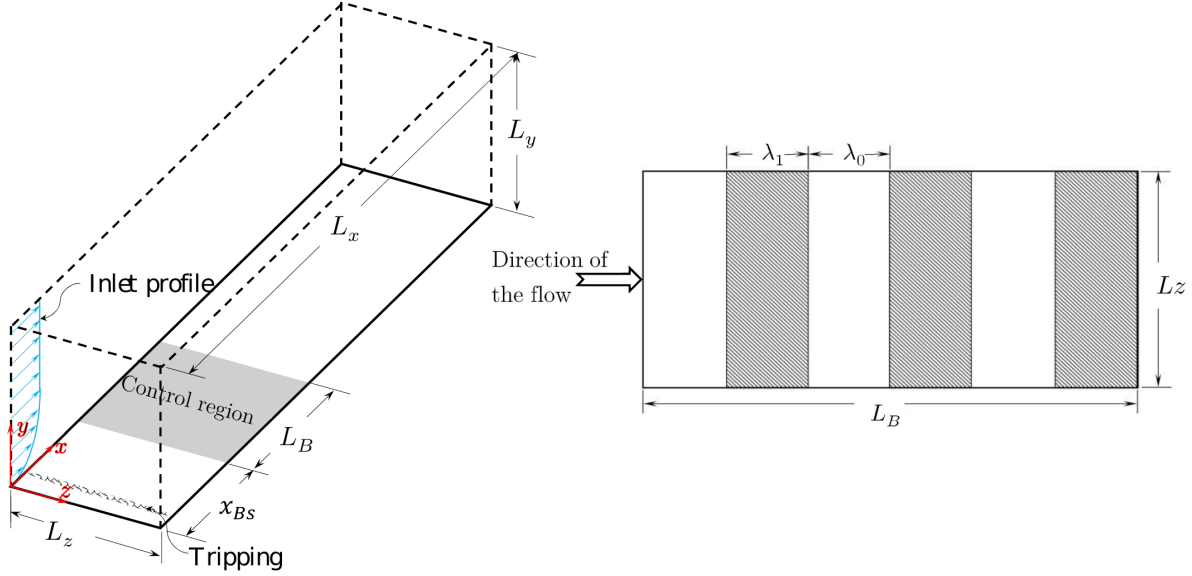


Figure 1: Left: Schematic of the computational domain. Grey shaded areas correspond to the control region. Right: Top-view of the control region.

Our numerical set-up is validated by comparing our data with the canonical TBL of Schlatter and Örlü [28] and the controlled TBL (using vertical wall blowing) of Stroh et al. [17]. The control region is located at a distance  $x_{Bs} = 76\delta_0$  from the inlet and has a streamwise extent  $L_B$  equal to  $85\delta_0$ , corresponding to  $470 \leq Re_\theta \leq 700$  of the canonical case. The blowing coefficient  $C_B = \frac{v_w}{U_\infty}$ , where  $v_w$  is the normal blowing velocity at wall, is equal to 0.005, which corresponds to a blowing intensity equal to 0.5% of the free stream velocity. Data are averaged in the spanwise direction and in time over  $T \sim 5000 \frac{\delta_0}{U_\infty}$ . Figure 2 shows that the streamwise evolution of the friction coefficient in our canonical TBL is in good agreement with the reference data of Schlatter and Örlü [28]. The friction coefficient is evaluated as follow

$$c_f(Re_\theta) = \frac{\tau_w(Re_\theta)}{0.5\rho U_\infty^2},$$

which is a function of  $Re_\theta$  for spatially developing flows. Here,  $\tau_w$  is the mean wall shear stress and  $\rho$  is the (constant) density of the fluid. It can be seen in figure 2 (right) that the mean streamwise velocity profiles and the root-mean-square velocity fluctuation profiles at  $Re_\theta = 1000$  (black lines) and  $Re_\theta = 1410$  (blue lines) for the canonical case are in good agreement with the reference data of Schlatter and Örlü [28]. As seen in figure 2 (left), the streamwise evolution of the friction coefficient for the controlled case is very similar to the one obtained in the reference data of Stroh et al. [17], with a maximum reduction of the shear stress of 56% at  $Re_\theta \sim 650$ . The only noticeable difference is the behaviour of the friction coefficient in the recovery region downstream of the control region. For

the reference data, the friction coefficient of the controlled case is similar to the friction coefficient of the canonical case from  $Re_\theta \sim 1300$  whereas in our simulation, the friction coefficient is always lower than the canonical one. This discrepancy may be attributed to the streamwise extent of the computational domain in the present simulations, which is much smaller than in the reference data. As already observed in the reference data of Stroh et al. [17], it can be concluded that low intensity uniform blowing at the wall reduces the skin-friction drag and that the boundary layer requires a relaxation distance to recover the canonical trend for the friction coefficient.

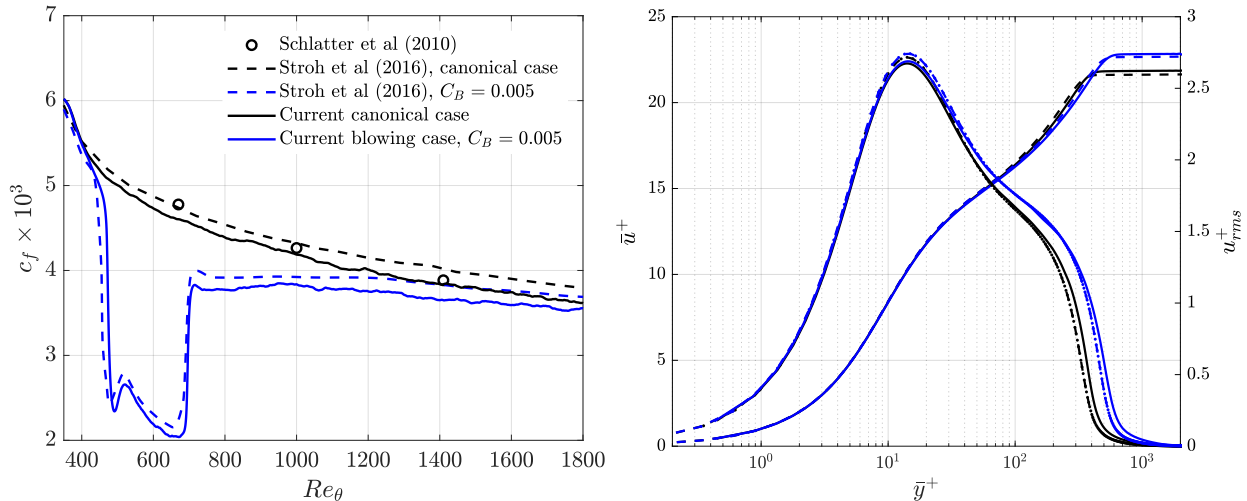


Figure 2: Left: streamwise evolution of the friction coefficient as a function of the Reynolds number  $Re_{theta}$  for the canonical and controlled cases. Right: mean and fluctuation streamwise velocity profiles at  $Re_\theta = 1000$  (black color) and  $Re_\theta = 1410$  (blue color). Solid lines correspond to the present results and the dashed lines to the reference data of Schlatter and Örlü [28].

### 3 Bayesian Optimisation algorithm

In the present study, a Bayesian Optimisation (BO) algorithm is used to achieve drag reduction and net-power saving. Generically, BO algorithms seek to minimize a chosen objective function over a given set of parameter values. BO algorithms have two stages. First, given knowledge of the objective at a known set of parameters, a probability density function for the objective function is computed. This encapsulates a *best guess* of the objective and quantifies the uncertainty of the approximation. Second, an *acquisition function* is minimized to determine the next set parameter values to be sampled. This typically involves a trade-off between minimizing the objective and reducing uncertainty of its approximation.

Specifically, consider an experiment with  $m$  input parameters, denoted  $\mathbf{x} \in \mathbb{R}^m$ , and a scalar-valued objective function  $f(\mathbf{x}) \in \mathbb{R}$  that we aim to minimize. Suppose that  $n$  experiments have been conducted at input values  $(\mathbf{x}_i)_{i=1}^n$  and that the objective function values  $f(\mathbf{x}_i)$  are known. Collecting these values as

$$X := \begin{bmatrix} \uparrow & & \uparrow \\ \mathbf{x}_1 & \cdots & \mathbf{x}_n \\ \downarrow & & \downarrow \end{bmatrix} \in \mathbb{R}^{m \times n}, \quad \mathbf{f} := \begin{bmatrix} f(\mathbf{x}_1) \\ \vdots \\ f(\mathbf{x}_n) \end{bmatrix} \in \mathbb{R}^n.$$

a *training set* is defined as  $\mathcal{D} := \{X, \mathbf{f}\}$ .

Our aim is to approximate the value of the objective function at a new *test set* of input values  $(\mathbf{x}_i^*)_{i=1}^q \subset \mathbb{R}^m$ . To achieve this, a BO methodology assumes a particular form of Gaussian uncertainty in the relation between input parameters  $\mathbf{x}$  and the objective function value  $f(\mathbf{x})$  (Rasmussen [30]). Under this assumption, the value of the objective at each test point  $\mathbf{x}_i^*$  is itself a random variable, which we denote  $f_i^*$ . Letting  $\mathbf{f}^* = (f_i^*)_{i=1}^q$  and  $X^* := [\mathbf{x}_1^*, \dots, \mathbf{x}_q^*] \in \mathbb{R}^{m \times q}$ , it can be shown that, given knowledge of the training set  $\mathcal{D}$  and chosen test inputs  $X^*$ ,

$$(\mathbf{f}^* | X^*, \mathcal{D}) \sim \mathcal{N}(\mu(X^*, \mathcal{D}), \sigma(X^*, \mathcal{D})).$$

That is, the unknown values of the objective function  $\mathbf{f}^*$  at testing points  $\mathbf{x}_i^*$  have a multivariate normal distribution with mean  $\mu = \mu(X^*, \mathcal{D})$  and covariance matrix  $\Sigma = \Sigma(X^*, \mathcal{D})$ . This distribution is commonly referred to as the *posterior*. Its mean and covariance are given by

$$\begin{aligned} \mu &= K(X^*, X)K(X, X)^{-1}\mathbf{f}, \\ \Sigma &= K(X^*, X^*) - K(X^*, X)K(X, X)^{-1}K(X, X^*), \end{aligned}$$

where  $K(A, B) \in \mathbb{R}^{\ell \times p}$  is a kernel matrix calculated from inputs  $A \in \mathbb{R}^{m \times \ell}$ ,  $B \in \mathbb{R}^{m \times p}$ . In this study, the elements of  $K(A, B)$  are chosen to be the *Matérn 5/2* kernels

$$K(A, B)_{ij} = k(\mathbf{a}_i, \mathbf{b}_j) = \theta_0 \left( 1 + \sqrt{\frac{5\|\mathbf{a}_i - \mathbf{b}_j\|_2}{l}} + \frac{5}{3} \frac{\|\mathbf{a}_i - \mathbf{b}_j\|_2^2}{l^2} \right) \exp \left( -\sqrt{\frac{5\|\mathbf{a}_i - \mathbf{b}_j\|_2}{l}} \right), \quad (1)$$

for  $i = 1, \dots, \ell, j = 1, \dots, p$ . Here,  $\theta_0$  is the covariance amplitude, and  $l$  is a length scale which determines the smoothness of the posterior.

The second stage of the BO algorithm is to select the next sample point  $\mathbf{x}_{n+1}$ , given the training set  $\mathcal{D}$  and the computed posterior distribution  $\mathbf{f}^*$ . This is performed by considering an acquisition function  $a(\mathbf{x})$ , which trades off between *exploitation* (to select the sample of the lowest mean) and *exploration* (to sample from a region of high uncertainty), and computing

$$\mathbf{x}_{n+1} = \operatorname{argmax}\{a(\mathbf{x}) : \mathbf{x} \in X^*\}.$$

While many acquisition functions have been proposed (Snoek et al. [20], Brochu et al. [21]), the one selected in this study is the *expected improvement* (EI). EI takes into account the probability of improvement, and the magnitude of the expected improvement, with respect to the best known value of the objective function  $f_{\text{best}} := \max_{\mathbf{x} \in X} f(\mathbf{x})$ , given knowledge of  $\mathcal{D}$ . In particular,

$$a(\mathbf{x}) = \sigma(\mathbf{x}|\mathcal{D}) [\gamma(\mathbf{x})\Phi(\gamma(\mathbf{x})) + \phi(\gamma(\mathbf{x}))], \quad \mathbf{x} \in X^*,$$

where

$$\gamma(\mathbf{x}) = \frac{\mu(\mathbf{x}|\mathcal{D}) - f_{\text{best}}}{\sigma(\mathbf{x}|\mathcal{D})}, \quad \mathbf{x} \in X^*,$$

and  $\phi(\cdot)$  and  $\Phi(\cdot)$  are the probability density function (PDF) and the cumulative distribution function (CDF), of a standard  $\mathcal{N}(0, 1)$  distribution, respectively.

For a simple illustrative example of the BO algorithm, consider a 1D problem that has a noise-free objective function,  $f(x) = \sin(x)/x$ , for  $-2 \leq x \leq 1$ . In this example, we fix the fitting parameters of (1) to be  $\theta_0 = 1$  and  $l = 0.8$ . Starting with an arbitrary input parameter  $x_1 = -1.5$  and corresponding training set  $\mathcal{D} = \{-1.5, f(-1.5)\}$ , figure 3 shows the development of the posterior distribution over five iterations of the BO algorithm.

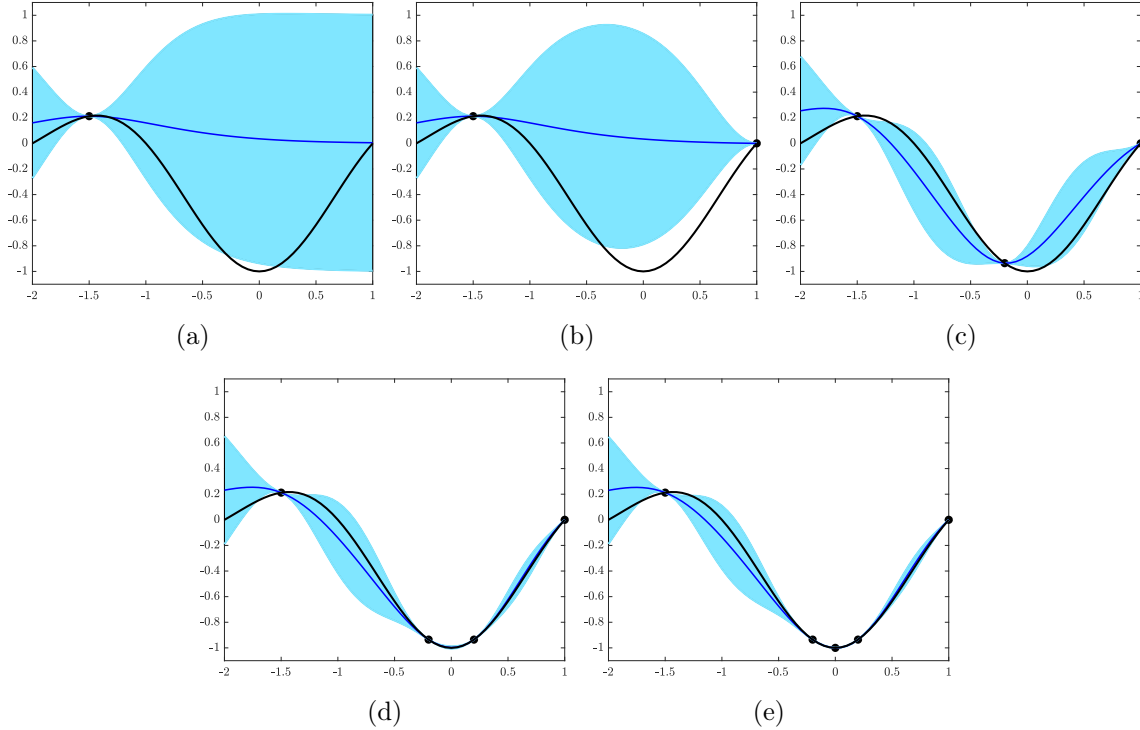


Figure 3: An example of using Bayesian Optimisation on 1D toy problem. The black curve is the true objective function, black markers are the observed points, the dark blue curve is posterior mean  $\mu$  and the blue shaded area the posterior uncertainty ( $\mu \pm \sigma$ ).

Near the training points (black markers), the posterior mean  $\mu$  (dark blue curve) and the true function (black curve) match and the posterior covariance  $\sigma$  vanishes; conversely, the uncertainty of the predictive model increases with distance from the observation points. With the EI acquisition function, the first new input parameter  $x_2$  shown in figure 3b corresponds to the lowest value of the posterior mean. Subsequently, since  $x_2$  is close to the lowest value of the new posterior mean (almost unchanged from the previous figure), the acquisition function selects a testing point  $x_3$  in a region of high uncertainty in figure 3c. This behaviour is repeated in figure 3d, after which the minimum of the posterior mean approximately coincides with the true optimum in figure 3e.

## 4 Parameters for the optimisation problem

Bayesian Optimisation of wall blowing control is implemented with the Matlab function `bayesopt` (see <https://uk.mathworks.com/help/stats/bayesopt.html>). The optimisation process can be parallelized, since multiple DNS can be performed at the same time to evaluate the objective function. For the present study, up to four simulations were performed at the same time using a total of up to 8,192 computational cores (each simulation runs for approximately 48 hours). As described in section 3, The *Matérn 5/2* kernel function and the EI acquisition function are used for this study. The blowing control region is similar to the one used in the validation case, from  $Re_\theta = 470$  to  $Re_\theta = 700$ , as seen in figure 1. The control region consists of alternating blowing and non-blowing areas. The streamwise length of a blowing area,  $\lambda_1$ , the streamwise length of a non-blowing areas,  $\lambda_0$ , and the blowing coefficient  $C_B$  are chosen as optimisation parameters. Note that the control region always

starts with a non-blowing area. An example is shown in figure 1 with three blowing areas and three non-blowing areas for the control region. To avoid spurious oscillations, the blowing is imposed gradually at the start and the end of each blowing area for a streamwise distance  $x \sim 4\delta_0$  using an hyperbolic tangent function. To account for this transition region (where  $C_B$  gradually increases), the optimisation process has the constraint  $\lambda_1 > 14$  imposed. Blowing and non-blowing areas are assumed to be repeated regularly in the control region, and optimisation variables are chosen to be the number of blowing areas  $n_B$  and the blowing-to-non-blowing area ratio  $\gamma = \lambda_1/\lambda_0$ . The parameters  $\lambda_0$  and  $\lambda_1$  may then be calculated in terms of the optimisation variables  $n_B$  and  $\gamma$ . For the present study, the range of these parameters are  $1 \leq n_B \leq 10$ ,  $0 \leq \gamma \leq 1$  and  $0 \leq C_B \leq 1$ .

In this study we are interested in the net-energy saving generated by a global drag reduction from  $35\delta_0$  to  $650\delta_0$  (corresponding to  $360 \leq Re_\theta \leq 1730$  in the canonical case). The region very close to the outlet (for  $Re_\theta > 1730$ ) is removed as the data in this region are contaminated by the outlet boundary condition. The global drag reduction is calculated using the mean friction coefficient  $C_f$  (global skin friction) over the streamwise length  $L = 615\delta_0$ ,

$$C_f = \frac{1}{L} \int_{35\delta_0}^{650\delta_0} c_f(x) dx. \quad (2)$$

The net-energy saving  $S$  is the ratio between the reduction of the total power coefficient due to wall blowing and the power coefficient of the uncontrolled case.

$$S = \frac{C_w - C_{w0}}{C_{w0}}, \quad (3)$$

where  $C_{w0}$  is the power coefficient of the canonical case. The gross power input coefficient for controlled case  $C_w = C_{w\tau} + C_{wb}$  is equal to the sum of the mean viscous power coefficient  $C_{w\tau}$  to overcome the shear stress, and the blowing power coefficient  $C_{wb}$  needed to inject flow through the permeable surface. The viscous power coefficient has the same value as the global friction coefficient,  $C_{w\tau} = C_f$ . The blowing power coefficient is equal to

$$C_{wb} = (C_p C_B + C_B^3) \alpha, \quad (4)$$

where  $\alpha$  is the ratio of the blowing region to the total area over which the global drag is calculated. Finally,  $C_p$  is the pressure coefficient of the pressure difference across the permeable wall  $\Delta p$  required for the fluid to flow through the surface

$$C_p = \frac{\Delta p}{\frac{1}{2}\rho U_\infty^2}. \quad (5)$$

Most numerical studies assume that  $C_p$  is equal to zero (Kametani et al. [16]). However,  $C_p$  could be significant with the potential to generate net-energy losses. Therefore, for the optimisation of the blowing parameters,  $C_p$  cannot be ignored. In order to evaluate the power required for the wall-blowing control system, the experimental set-up of Kornilov and Boiko [1] is used as a proxy. In this experimental work performed in a low-turbulence wind tunnel, a permeable material of porosity equal to 17.1% was used to generate wall-blowing with an average pore orifice diameter of 0.17 mm, a wall thickness of 1.1 mm, and an orifice aspect ratio 6.47. These geometric characteristics were chosen because such a configuration of orifices was found to be promising with respect to skin-friction drag reduction. Such a blowing system can easily be reproduced numerically by simply imposing a uniform vertical velocity  $v_w$  at the wall of the boundary layer in the control region. Fortunately, experimental data are available for the variation of the pressure coefficient  $C_p$  as a

function of the blowing coefficient  $C_B$  (see figure 11 in Kornilov and Boiko [1]). Interestingly, the relation between  $C_p$  and  $C_B$  is linear,  $C_p = 124 C_B$ . This relation is used in the present study to evaluate the blowing power coefficient. In addition to the injected mass flow rate, the pressure drop is also function of the porosity, hole diameter and plate thickness. Therefore, this relation is particular to the permeable plate used by Kornilov and Boiko [1], and would differ for other designs, potentially facilitating greater power saving with a more efficient blowing device.

In order to evaluate the objective function, i.e. the net-energy saving given by (3), several DNS of a TBL are performed with various blowing parameters. For each evaluation, the simulation runs for  $T = 1600 \frac{\delta_0}{U_\infty}$ . For the first half of this time, the flow adapts to the wall blowing condition, and then the statistics are collected for the second half on the simulation window. It is found that  $T = 800 \frac{\delta_0}{U_\infty}$  is enough to have a good estimate of the friction coefficient and the net-energy saving with an error margin of  $\pm 1\%$ . If the preliminary estimation of the net-energy saving is less than 2.5%, data are collected over an extra  $T = 1600$  to reduce the error margin.

## 4.1 Results and Discussion

In total, 18 DNS simulations are conducted for the present Bayesian Optimisation study (to be compared with the canonical case). The blowing parameters for the first three simulations are selected arbitrarily (to pre-test the behaviour of wall blowing) and are used to initialize the Bayesian Optimisation. The parameters of the remaining 15 simulations are determined by the optimisation algorithm. Table 1 shows the parameters used for each run, the corresponding global friction coefficient of the area  $360 \leq Re_\theta \leq 1730$  and the net-power saving. Case 0 corresponds to the canonical case. Figure 4 (left) shows the local friction coefficient as function of the  $Re_\theta$  for all the cases. Substantial drag reductions is observed for all simulations, especially over the control region, and only the parameters in case 11 generate a global drag increase. It should be noted that the Bayesian Optimisation algorithm converges to a uniform blowing strategy over the control region, corresponding to  $\lambda_0 = 0$ , which is evident from case 13 onwards. As anticipated, increased blowing intensity corresponds to increased drag reduction but not necessarily increased power saving. Indeed, the largest observed drag reduction of 18.9% in case 5 has an energy loss of 20.8% compared to the canonical case. The highest net-power saving is obtained in case 13 with a net-power saving of 5%, corresponding to a relatively low reduction of 8.3% of the friction coefficient. As previously discussed, higher net-power saving can be achieved with a more efficient blowing device, so this preliminary result is potentially very interesting for the future. It is important to point out that if an idealised control power was used (i.e ignoring the effect of the pressure needed for the blowing device) the Bayesian Optimisation algorithm would have a different search path, with potentially misleading conclusions. Note also that blowing is applied at fairly low Reynolds numbers, and as pointed out by Kametani and Fukagata [15], for the same blowing ratio  $v_w/U_\infty$ , the drag reduction could potentially increase for higher  $Re$ . In the remaining of this section, we will focus on three cases: case 0 which is the uncontrolled case (black lines), Case 5 (red lines) with the highest global drag reduction and the highest power loss and Case 13 (blue lines) which has the highest net-energy saving.

Wall blowing distorts and accelerates the growth rate of the TBL with a jump in the boundary layer thickness at the start of the control region as seen in figure 4 (right). With low blowing velocity (Case 13,  $C_B = 0.289$ ) the distortion of the boundary layer thickness at the beginning of the blowing region is less important when compared to case 5 with  $C_B = 0.997$ . Downstream of the control region, the friction coefficient eventually recovers to its uncontrolled values, however with a higher boundary layer thickness. This result was already observed in Stroh et al. [17] and it was concluded that the increase of the boundary layer thickness downstream of the control region can

Case number	$C_B$	$\lambda_1 (\times \delta_0)$	$\lambda_0 (\times \delta_0)$	Global Drag Reduction	Net Power Saving S
0	0	—	—	0	0
1	0.5	85	0	13.2	3.2
2	0.5	40	45	6.0	1.3
3	0.5	20	65	2.9	0.6
4	0.37	17	0.3	9.3	3.8
5	0.997	8.5	0.3	18.9	-20.8
6	0.032	84.7	0.6	0.9	0.9
7	0.424	97	0.3	11.0	3.8
8	0.404	23	0.3	9.6	3.1
9	0.233	10.5	0.3	5.4	3.3
10	0.136	5	80	0.4	0.3
11	0.0003	8	0.9	-0.5	-0.5
12	0.59	8.5	0.3	12.3	-1.6
13	0.289	85	0	8.3	5.0
14	0.386	85	0	10.4	4.5
15	0.296	85	0	8.4	4.8
16	0.29	85	0	8.1	4.8
17	0.289	85	0	7.9	4.6
18	0.278	85	0	7.6	4.5

Table 1: Blowing parameters for each simulation and the corresponding global drag reduction (in %) and net-power saving.

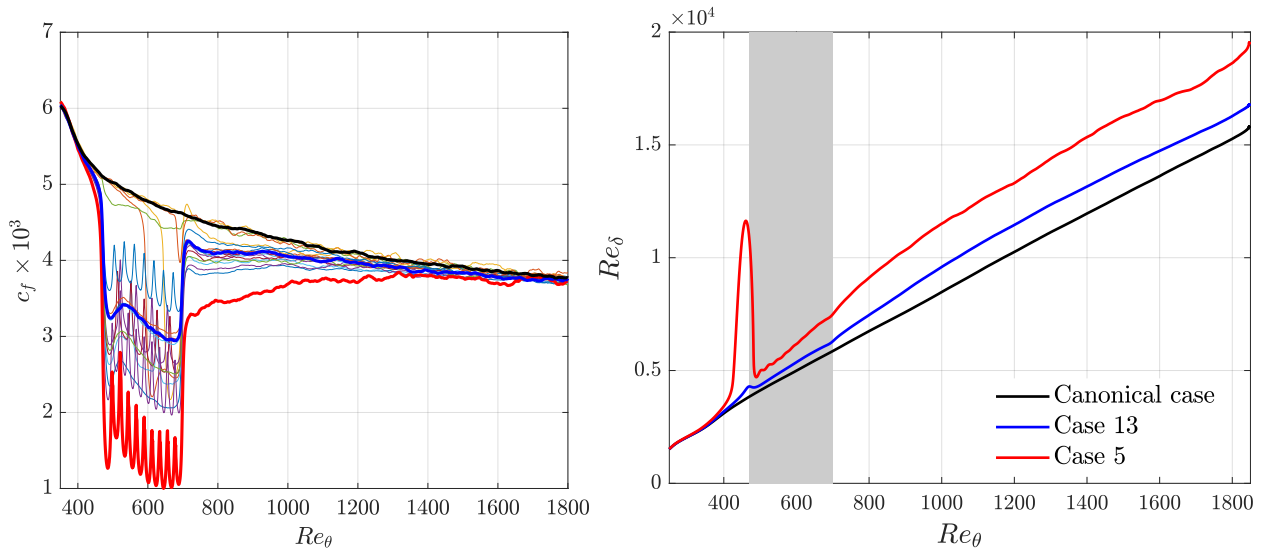


Figure 4: Left: Streamwise evolution of the friction coefficient as a function of  $Re_\theta$  for all the cases. The thick solid lines corresponds to the three cases of interest in this study: Case 0 (black), Case 13 (blue) and Case 5 (red). Right: Streamwise evolution of  $Re_\delta$  (based on the boundary layer thickness) for the uncontrolled case, Case 5 and Case 13. The blowing section is highlighted in grey.

be described by a streamwise shift of the virtual origin of the turbulent boundary layer. It means that uniform blowing can potentially be advantageous at significant distances downstream of the control region because it yields not only a significant drag reduction in the blowing region, but also

a greater boundary layer thickness downstream of the control region with lower wall friction.

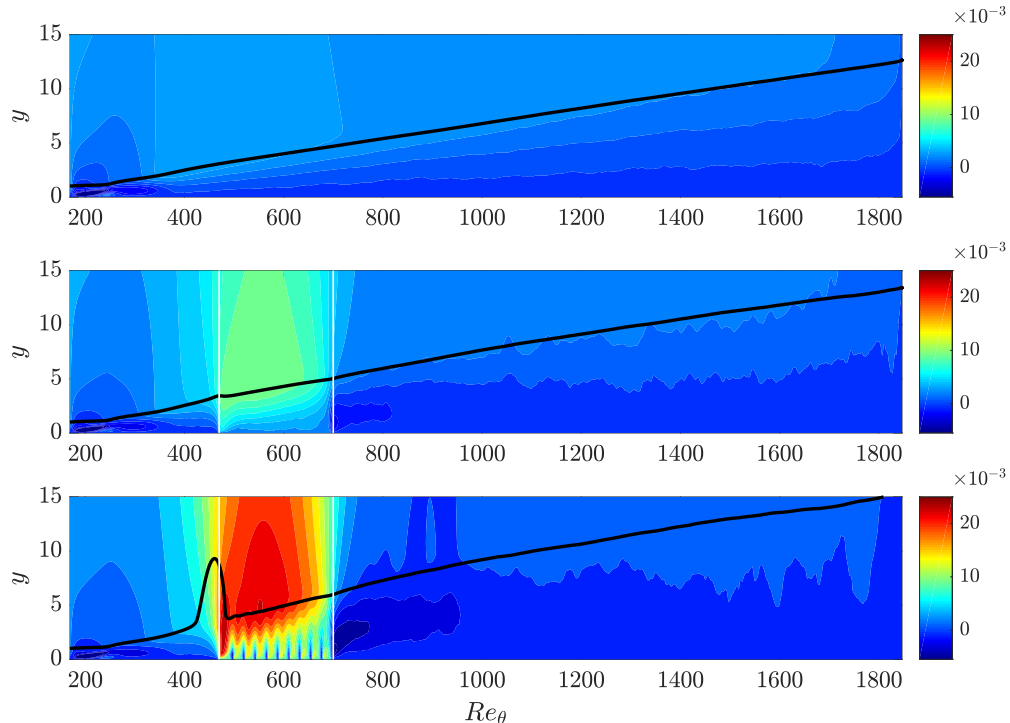


Figure 5: Contours of the mean normal velocities of the cases, from the top, Case 0, Case 13 and Case 5. The black line is the boundary layer thickness where  $u = 0.99U_\infty$ . Here, the velocities are normalized by  $U_\infty$ , and  $y$  and  $x$  are normalized by  $\delta_0$

Other interesting features related to blowing control can be observed in figure 5 where the mean normal velocity is plotted for cases 0, 5 and 13. Over the control region, it can be seen that the normal velocity is typically much higher than the blowing velocity at the wall  $v_w$ . This can be related to a strong adverse pressure gradient just upstream of the blowing. The streamwise velocity is blocked and deflected upwards, increasing the normal velocity over the control region. Downstream of the control region, a favourable pressure gradient is present. As a result, negative values for the normal velocity can be observed associated with lower values for the friction coefficient downstream of the blowing when compared to the canonical case. These adverse and favourable pressure gradients when starting and stopping the blowing were also reported in Kametani et al. [18]. Consistently with the literature, wall blowing enhances turbulence which is then convected downstream and promotes the Reynolds shear stress as seen in figure 6. The magnitude of Reynolds shear stress increases with the blowing intensity. Note also that the tripping is clearing visible in figure 5 for  $Re_\theta \sim 200$ .

## 5 FIK identity analysis of skin friction drag

Fukagata et al. [14] derived an expression of the skin-friction coefficient for incompressible turbulent flows. Their expression is known as the Fukagata-Iwamoto-Kasagi (FIK) identity. For spatially developing boundary layers which are homogeneous in the spanwise direction, the FIK identity can

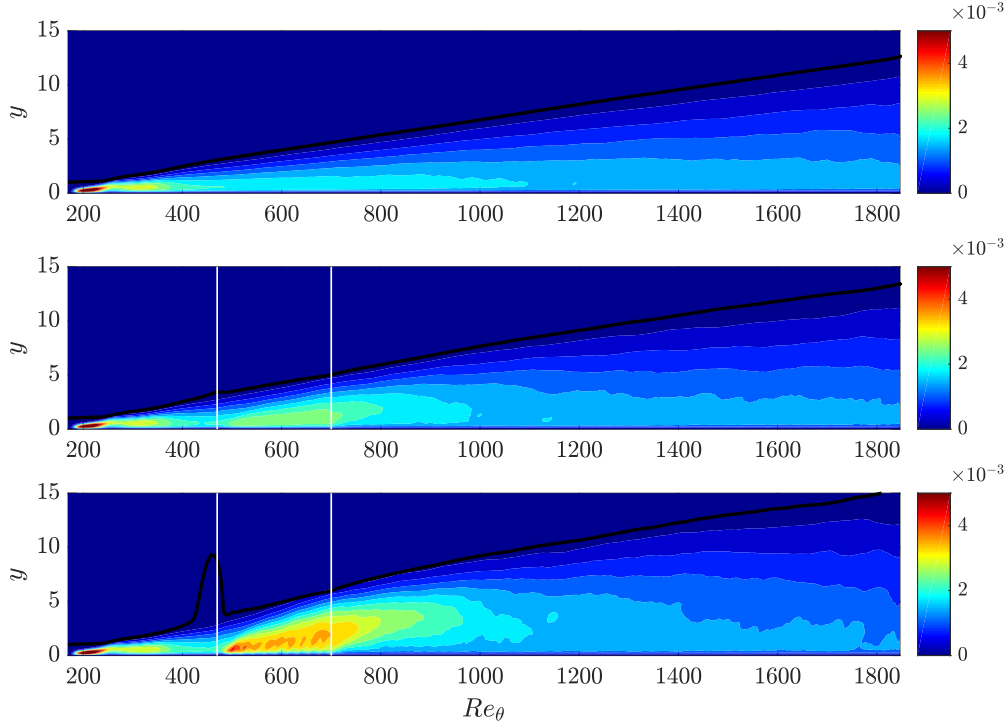


Figure 6: Contours of the Reynolds shear stress of the cases, from the top, Case 0, Case 13 and Case 5. The black line is the boundary layer thickness where  $u = 0.99U_\infty$ . Here, the velocities are normalized by  $U_\infty$ , and  $y$  and  $x$  are normalized by  $\delta_0$

be expressed as

$$\begin{aligned}
 c_f^{FIK}(x) = & \underbrace{\frac{4(1 - \delta^*)}{Re_\delta}}_{c_f^\delta} + 4 \underbrace{\int_0^1 (1 - y)(-\overline{u'v'})dy}_{c_f^T} + 4 \underbrace{\int_0^1 (1 - y)(-\overline{uv})dy}_{c_f^C} \\
 & - 2 \underbrace{\int_0^1 (1 - y)^2 \left( \frac{\partial \overline{u\overline{u}}}{\partial x} + \frac{\partial \overline{u'u'}}{\partial x} - \frac{1}{Re_\delta} \frac{\partial^2 \overline{u}}{\partial x^2} + \frac{\partial \overline{p}}{\partial x} \right) dy}_{c_f^D},
 \end{aligned} \tag{6}$$

where  $\overline{\cdot}$  denotes the Reynolds-averaged quantities,  $\delta^*$  is the displacement thickness and  $Re_\delta = \frac{U_\infty \delta}{\nu}$ . All the dimensions,  $\delta^*$ ,  $x$  and  $y$  are normalized by the local boundary layer thickness  $\delta$ . For the present study, it is assumed that  $\frac{\partial \overline{p}}{\partial x} = 0$ . The FIK identity decomposes the friction coefficient into four terms: a contribution from boundary layer thickness  $c_f^\delta$ , a Reynolds shear stress contribution  $c_f^T$ , a mean wall-normal convection contribution  $c_f^C$  and a spatial development contribution  $c_f^D$ . The spatial development contribution  $c_f^D$  consists of four terms

$$\begin{aligned}
 c_f^D = & c_f^{D1} + c_f^{D2} + c_f^{D3} + c_f^{D4} \\
 = & -2 \int_0^1 (1 - y)^2 \left( \frac{\partial \overline{u\overline{u}}}{\partial x} + \frac{\partial \overline{u'u'}}{\partial x} - \frac{1}{Re_\delta} \frac{\partial^2 \overline{u}}{\partial x^2} + \frac{\partial \overline{p}}{\partial x} \right) dy.
 \end{aligned} \tag{7}$$

Note that the mean wall-normal convection term and the spatial development term are absent in fully developed channel and pipe flows. For a more detailed discussion about each term of the FIK identity for spatially evolving boundary layers, see Kametani and Fukagata [15].

Figure 7 shows that the friction coefficient calculated by the streamwise shear stress,  $c_f$ , matches the one calculated by the FIK identity,  $c_f^{FIK}$ , for the canonical case. The agreement is also very good for cases 5 and 13 downstream of the blowing region and differences can be observed over the blowing region. For the canonical case, it can be seen that the main contributions to the the skin friction coefficient are  $c_f^T$  and  $c_f^D$  while  $c_f^C$  has a significant negative contribution. The less dominant contribution is  $c_f^\delta$  with a slowly decreasing contributions which will eventually reaches zero for very large Reynolds numbers.

When wall blowing is applied,  $c_f^{FIK}$  deviates from  $c_f$  over and near the blowing area in agreement with previous simulations in a similar set-up (Kametani and Fukagata [15]). The deviation is very pronounced at the beginning and the end of the blowing region for case 5 as a result of the adverse and favourable pressure gradients reported in the previous section and not taken into account in the FIK identity for the present study. For case 13, where uniform blowing is applied with a relatively low blowing intensity ( $C_B = 0.289$ ), the difference between  $c_f^{FIK}$  and  $c_f$  is reasonable in the middle of the blowing region. For case 5, because of the discrete blowing areas within the blowing region, the FIK identity as defined in the present study does not produce a correct estimation of the friction coefficient over the blowing region. This problem should be easily corrected by introducing an extra term related to the streamwise evolution of the pressure in the FIK identity. For the intermittent blowing case, it is interesting to notice that the Reynolds shear stress contribution is not sensitive to the intermittency of the blowing whereas the spatial development contribution  $c_f^D$  and mean convection contribution  $c_f^D$  are oscillating and nearly cancelling each other.

For all cases, the spatial development contribution  $c_f^D$  is clearly dominated by the spatial development of the streamwise velocity gradient as seen in figure 8. The remaining terms,  $c_f^{D2}$  and  $c_f^{D3}$  are virtually zero for the canonical case. It should be noted, however, that  $C_f^{D2}$  exhibits small oscillations around zero at the start and end of blowing regions. Interestingly,  $c_f^D$  increases significantly downstream of the wall blowing with positive values for case 13 and negative values for case 5.

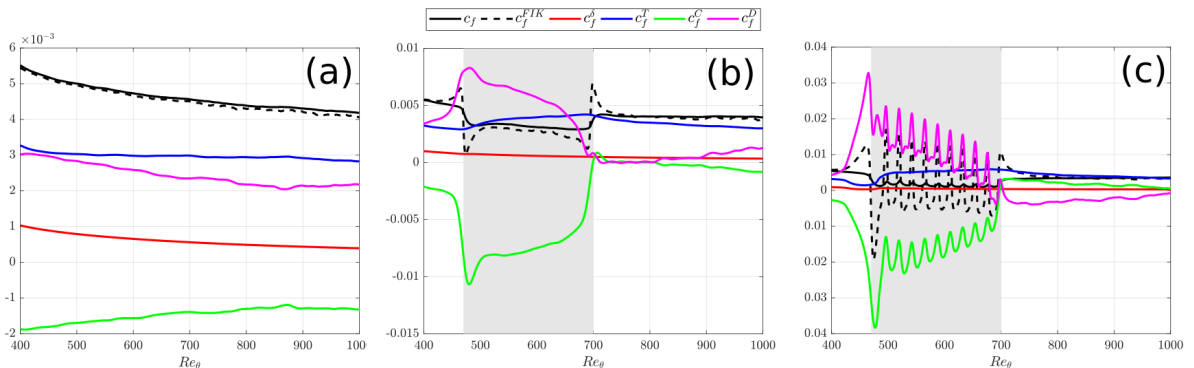


Figure 7: Streamwise evolution of the terms from the FIK decomposition for (a) Case 0, (b) Case 13 and (c) Case 5.

An intriguing observation is related to the mean convection contribution which is positive for case 5 and negative for case 13 downstream of the blowing region. It might be related to the presence of strong values for the Reynolds shear stress in the blowing region for case 5. To obtain drag reduction, the increase for  $c_f^D$  and  $c_f^T$  needed to be counteracted by a strong reduction for  $c_f^C$ .

The significant growth of the magnitude of  $c_f^C$  is mainly due to the increase of the mean normal velocity in the blowing section (see figure 5). In Case 13,  $c_f^D$  grows rapidly at the beginning of the blowing region, but then decays gradually over the blowing area reaching very small values before slowly converging to the value observed in the canonical case. For case 5,  $C_f^D$  oscillates along the blowing region, but drops to negative values after the control section, while  $c_f^C$  becomes positive after the control section. Therefore, it is possible to conclude that over the blowing region the reduction of the convection contribution  $c_f^C$  is responsible for the total drag reduction, while the spatial development contribution  $c_f^D$  is responsible for the low drag observed downstream of the blowing region.

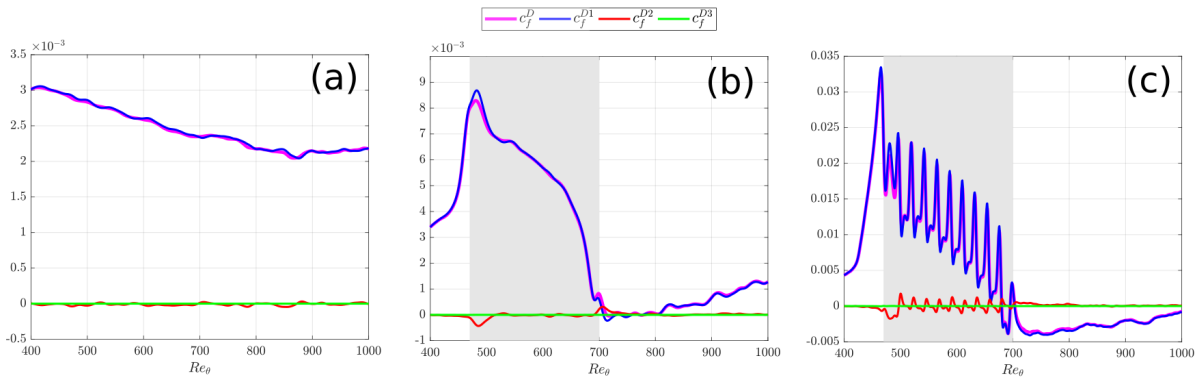


Figure 8: Streamwise evolution of the terms associated to the spatial development contribution term for (a) Case 0, (b) Case 13 and (c) Case 5.

## 6 Conclusion and Future Work

In this work, DNS of a specially developing turbulent boundary layer with continuous/discontinuous wall blowing were performed to provide data for a Bayesian Optimisation algorithm and used to find the optimal parameters to reduce the friction coefficient of the boundary layer as well as generating net-power saving. Net-energy saving was estimated based on the global drag reduction over a large extend of the computational domain ( $365 \leq Re_\theta \leq 1730$ ) and the experimental data of Kornilov and Boiko [1] for an accurate estimation of the power required to generate the wall blowing. After 13 simulations, the Bayesian Optimisation algorithm converged to a control strategy corresponding to low intensity uniform blowing over the control region. An additional 5 simulations were performed but no significant improvements were made. A net-power saving of 5% was observed for the best set of parameters, corresponding to a blowing intensity 0.289% of the free stream velocity.

The results are very promising and future studies will address the relatively low net-energy saving by increasing the streamwise extent of the control region, by increasing the Reynolds numbers of the simulations and by increasing the number of parameters for the Bayesian Optimisation algorithm. Instead of using costly DNS, future studies will be based on Implicit Large-Eddy Simulations (ILES) which will allow for a longer computational domain to be employed and for a much larger number of simulations to be performed. Recently, a new method was implemented in |Incompact3d| in order to perform ILES. It is based on a strategy that introduces a targeted numerical dissipation at the small scales through the discretisation of the second derivatives of the viscous terms (Lamballais et al. [31], Dairay et al. [32]). It was shown in these studies that it is possible to design a high-order finite-difference scheme in order to mimic a subgrid-scale model for LES based on the concept of

Spectral Vanishing Viscosity (SVV, see for instance Tadmor [33], Karamanos and Karniadakis [34]), at no extra computational cost. ILES of a turbulent channel flow have already been performed with |Incompact3d| (Lamballais et al. [31]) so there should be no issue with turbulent boundary layers.

## Acknowledgements

The authors would like to thank EPSRC for the computational time made available on the UK supercomputing facility ARCHER via the UK Turbulence Consortium (EP/L000261/1). The authors also acknowledge PRACE for awarding them access to Marconi at CINECA, Italy (project 2016163847). Omar Mahfoze would like to thank Imperial College for funding his PhD with an Imperial College President Scholarship.

## References

- [1] Vladimir I Kornilov and Andrey V Boiko. Efficiency of air microblowing through microperforated wall for flat plate drag reduction. *AIAA journal*, 50(3):724–732, 2012.
- [2] Michael D Graham. Drag reduction and the dynamics of turbulence in simple and complex fluids. *Physics of Fluids*, 26(10):625–656, 2014.
- [3] Maurizio Quadrio and Pierre Ricco. Critical assessment of turbulent drag reduction through spanwise wall oscillations. *Journal of Fluid Mechanics*, 521:251–271, 2004.
- [4] P Dawes and H Wheeler. Preliminary experiments on sweat cooling. *Jet Propulsion Lab./California Institute of Technology Progress Report*, pages 3–13, 1946.
- [5] HS Mickley, RoCo Ross, AoLo Squyers, and WE Stewart. Heat, mass, and momentum transfer for flow over a flat plate with blowing or suction. Technical report, Massachusetts Inst. of Tech., 1953.
- [6] Morris W Rubesin. An analytical estimation of the effect of transpiration cooling on the heat-transfer and skin-friction characteristics of a compressible, turbulent boundary layer. *NACA TN 3341*, 1954.
- [7] Kaoru Torii, Niichi Nishiwaki, and Masaru Hirata. Heat transfer and skin friction in turbulent boundary layer with mass injection. In *Proceedings of the Third International Heat Transfer Conference*, volume 3, pages 34–48. Am. Inst. Chem. Engrs New York, 1966.
- [8] Roger L Simpson, RJ Moffat, and WM Kays. The turbulent boundary layer on a porous plate: experimental skin friction with variable injection and suction. *International Journal of Heat and Mass Transfer*, 12(7):771–789, 1969.
- [9] Yasushi Sumitani and Nobuhide Kasagi. Direct numerical simulation of turbulent transport with uniform wall injection and suction. *AIAA journal*, 33(7):1220–1228, 1995.
- [10] Joongnyon Kim, Kyoungyoun Kim, and Hyung Jin Sung. Wall pressure fluctuations in a turbulent boundary layer after blowing or suction. *AIAA journal*, 41(9):1697–1704, 2003.
- [11] Danny Hwang. An experimental study of turbulent skin friction reduction in supersonic flow using a microblowing technique. In *38th Aerospace Sciences Meeting and Exhibit*, page 545, 1999.

- [12] Danny Hwang. Review of research into the concept of the microblowing technique for turbulent skin friction reduction. *Progress in Aerospace Sciences*, 40(8):559–575, 2004.
- [13] Vladimir I Kornilov and Andrey V Boiko. Flat-plate drag reduction with streamwise noncontinuous microblowing. *AIAA journal*, 52(1):93–103, 2013.
- [14] Koji Fukagata, Kaoru Iwamoto, and Nobuhide Kasagi. Contribution of reynolds stress distribution to the skin friction in wall-bounded flows. *Physics of Fluids*, 14(11):L73–L76, 2002.
- [15] Yukinori Kametani and Koji Fukagata. Direct numerical simulation of spatially developing turbulent boundary layers with uniform blowing or suction. *Journal of Fluid Mechanics*, 681:154–172, 2011.
- [16] Yukinori Kametani, Koji Fukagata, Ramis Örlü, and Philipp Schlatter. Effect of uniform blowing/suction in a turbulent boundary layer at moderate reynolds number. *International Journal of Heat and Fluid Flow*, 55:132–142, 2015.
- [17] A Stroh, Y Hasegawa, Philipp Schlatter, and B Frohnapfel. Global effect of local skin friction drag reduction in spatially developing turbulent boundary layer. *Journal of Fluid Mechanics*, 805:303–321, 2016.
- [18] Yukinori Kametani, Koji Fukagata, Ramis Örlü, and Philipp Schlatter. Drag reduction in spatially developing turbulent boundary layers by spatially intermittent blowing at constant mass-flux. *Journal of Turbulence*, 17(10):913–929, 2016.
- [19] Michael A Gelbart, Jasper Snoek, and Ryan P Adams. Bayesian optimization with unknown constraints. *arXiv preprint arXiv:1403.5607*, 2014.
- [20] Jasper Snoek, Hugo Larochelle, and Ryan P Adams. Practical bayesian optimization of machine learning algorithms. In *Advances in neural information processing systems*, pages 2951–2959, 2012.
- [21] Eric Brochu, Vlad M Cora, and Nando De Freitas. A tutorial on bayesian optimization of expensive cost functions, with application to active user modeling and hierarchical reinforcement learning. *arXiv preprint arXiv:1012.2599*, 2010.
- [22] Chaitanya Talnikar, Patrick Blonigan, Julien Bodart, and Qiqi Wang. Parallel optimization for large eddy simulations. *arXiv preprint arXiv:1410.8859*, 2014.
- [23] Sylvain Laizet and Ning Li. Incompact3d: a powerful tool to tackle turbulence problems with up to o (105) computational cores. *International Journal for Numerical Methods in Fluids*, 67(11):1735–1757, 2011.
- [24] Sanjiva K Lele. Compact finite difference schemes with spectral-like resolution. *Journal of computational physics*, 103(1):16–42, 1992.
- [25] Sylvain Laizet and Eric Lamballais. High-order compact schemes for incompressible flows: A simple and efficient method with quasi-spectral accuracy. *Journal of Computational Physics*, 228(16):5989–6015, 2009.
- [26] Carlos Diaz-Daniel, Sylvain Laizet, and J Christos Vassilicos. Wall shear stress fluctuations: Mixed scaling and their effects on velocity fluctuations in a turbulent boundary layer. *Physics of Fluids*, 29(5):055102, 2017.

- [27] Carlos Diaz-Daniel, Sylvain Laizet, and J Christos Vassilicos. Direct numerical simulations of a wall-attached cube immersed in laminar and turbulent boundary layers. *International Journal of Heat and Fluid Flow*, 68:269–280, 2017.
- [28] Philipp Schlatter and Ramis Örlü. Assessment of direct numerical simulation data of turbulent boundary layers. *Journal of Fluid Mechanics*, 659:116–126, 2010.
- [29] Javier Jiménez, Sergio Hoyas, Mark P Simens, and Yoshinori Mizuno. Turbulent boundary layers and channels at moderate reynolds numbers. *Journal of Fluid Mechanics*, 657:335, 2010.
- [30] Carl Edward Rasmussen. Gaussian processes in machine learning. In *Advanced lectures on machine learning*, pages 63–71. Springer, 2004.
- [31] Eric Lamballais, Véronique Fortuné, and Sylvain Laizet. Straightforward high-order numerical dissipation via the viscous term for Direct and Large Eddy Simulation. *Journal of Computational Physics*, 230(9):3270–3275, 2011.
- [32] T. Dairay, E. Lamballais, S. Laizet, and J.C. Vassilicos. Numerical dissipation vs. subgrid-scale modelling for Large Eddy Simulation. *Journal of Computational Physics*, 337:252–274, 2017.
- [33] E. Tadmor. Convergence of spectral methods for nonlinear conservation laws. *SIAM Journal on Numerical Analysis*, 26(1):30–44, 1989.
- [34] G.S. Karamanos and G.E. Karniadakis. A spectral vanishing viscosity method for Large-Eddy Simulations. *Journal of Computational Physics*, 163(1):22–50, 2000.